DELPHI Collaboration DELPHI 99-29 CONF 228
8 March, 1999

Search for R-parity violation with a $\bar{U}\bar{D}\bar{D}$ coupling at $\sqrt{s} = 183$ GeV

R. Barbier [1], P. Jonsson [1], S. Katsanevas [1], N. Vassilopoulos [2]
[1]IPN, Lyon (France), [2]University of Oxford, Oxford (England)

Abstract

Searches for pair production of gauginos and sfermions in e^+e^- collisions at a center of mass energy of 183 GeV have been performed on data corresponding to an integrated luminosity of 53 pb^{-1} collected by the DELPHI detector at LEP. The data was analysed under the assumption of non-conservation of R-parity through a single dominant $\bar{U}\bar{D}\bar{D}$ coupling between squarks and standard quarks. Typical final states contain between 4 and 10 jets with or without additional leptons. No excess of data above Standard Model expectations was observed. The results were used to constrain domains of the MSSM parameter space and to derive limits on the masses of supersymmetric particles.

Mass limits from these searches;

- Neutralinos mass limit : $m_{\tilde{\chi}_1^0} \geq 21$ GeV
- Charginos mass limit : $m_{\tilde{\chi}_1^+} \geq 87$ GeV
- Stop and Sbottom mass limit (indirect decay) : for $\Delta M \geq 5$ GeV
  - $m_{\tilde{t_1}} \geq 62.5$ GeV, for $\Phi_{mix} = 0$ rad
  - $m_{\tilde{t_1}} \geq 49$ GeV, for $\Phi_{mix} = 0.98$ rad
  - $m_{\tilde{b_1}} \geq 58.5$ GeV, for $\Phi_{mix} = 0$ rad
- Selectrons mass limit for $\Delta M \geq 5$ GeV
  - $m_{\tilde{e_R}} \geq 70$ GeV
  - $m_{\tilde{e_L}} \geq 53$ GeV
- Smuons mass limit for $\Delta M \geq 5$ GeV and for $\tilde{\chi}_1^0 \geq 21$ GeV
  - $m_{\tilde{\mu_R}} \geq 68$ GeV
  - $m_{\tilde{\mu_L}} \geq 69$ GeV

1 Introduction

1.1 The R-parity violating Lagrangian

The most general way to write a superpotential including the symmetries and particle content of the Minimal Supersymmetric extension of the Standard Model (MSSM) [1] is:

$$W = W_{MSSM} + W_{RPV} \tag{1}$$

where W_{MSSM} represents interactions between MSSM particles consistent with $B - L$ conservation (B = baryon number, L = lepton number) and W_{RPV} describes interactions violating B or L conservation. These latter terms of the superpotential can explicitly be written as [3]:

$$\lambda_{ijk} L_i L_j \bar{E}_k + \lambda'_{ijk} L_i Q_j \bar{D}_k + \lambda''_{ijk} \bar{U}_i \bar{D}_j \bar{D}_k \tag{2}$$

where i, j and k are the generation indices[1]; L and $\bar{E}$ denote the left-handed doublet lepton and the right-handed singlet charge-conjugated lepton superfields respectively, whereas Q, $\bar{U}$ and $\bar{D}$ denote the left-handed doublet quark and the right-handed singlet charge-conjugated up- and down-type quark superfields; λ_{ijk}, λ'_{ijk} and λ''_{ijk} are the Yukawa couplings. The first two terms violate L conservation, and the third one B conservation. Since $\lambda_{ijk} = -\lambda_{jik}$, $\lambda''_{ijk} = -\lambda''_{ikj}$, there are 9 λ_{ijk}, 27 λ'_{ijk} and 9 λ''_{ijk} leading to 45 new couplings.

R-parity, where $R = (-1)^{3B+L+2S}$ for a particle with spin S [2], can be introduced as a symmetry violated by these couplings but conserved by W_{MSSM}. Standard model particles then have even R-parity, and their corresponding superpartners have odd R-parity. The magnitude of individual R-parity violating ($\not{R}_p$) couplings are constrained by various experimental and theoretical arguments (see chapter 1.2) but the simultaneous presence of both B and L violating $\not{R}_p$couplings is prohibited by requirements on the proton lifetime [4, 5].

One major phenomenological consequence of $\not{R}_p$ is that the Lightest Supersymmetric Particle (LSP) is allowed to decay to standard fermions. This fact modifies the signatures of the supersymmetric particle production compared to the expected signatures in case of R-parity conservation. In this paper, searches for pair produced neutralinos ($\widetilde{\chi}_i^0$), charginos ($\widetilde{\chi}^{\pm}$) and sfermions ($\widetilde{q}$, $\widetilde{\mu}$ and $\widetilde{e}$) was performed under the hypothesis of R-parity violation with one single dominant $\bar{U}\bar{D}\bar{D}$ coupling. $\bar{U}\bar{D}\bar{D}$ terms couple squarks to standard model quarks and the experimental signature of the $\not{R}_p$events thus becomes multiple hadronic jets, and in most of the cases without missing energy.

1.2 Pair production of gauginos and sfermions

Pair production of supersymmetric particles with $\not{R}_p$ is similar to standard $R_p$conserved pair production since the $\bar{U}\bar{D}\bar{D}$ couplings does not enter in the vertex.

The mass spectrum of neutralinos and charginos is fixed in this analysis by the three parameters of the MSSM theory assuming GUT scale unifiaction of gaugino masses : M_2, the SU(2) gaugino mass parameters at the electroweak scale, μ, the mixing mass term of

[1] An additional fourth term in eq.2, describing a bilinear coupling between the left handed lepton superfield and the up-type Higgs field, is usually assumed to be zero.

the Higgs doublets at the electroweak scale and $tan\beta$, the ratio of the vacuum expectation values of the two Higgs doublets. The neutralinos and charginos are pair-produced either in the s-channel via a γ or a Z or in the t-channel exchange of a selectron (sneutrino) for the neutralinos (charginos) (figure 1). Depending on the values of the different parameters, the cross sections at $\sqrt{s} = 183$ GeV vary typically from 0.1 to 10 pb.

The pair production of charged sleptons ($\tilde{e}$ and $\tilde{\mu}$) and squarks ($\tilde{q}$) is also studied in this paper. Sfermion masses are obtained from m_0, the common scalar mass at the GUT scale, and for the third generation from the left-right mixing angle. The members of the third generation ($\tilde{t}$, $\tilde{b}$, $\tilde{\tau}$) are the most likely candidates for light sfermions due to their potential for large mixing angles and their large Yukawa coupling.

The sfermions of the two last generations can be produced via the exchange in the s-channel of a Z (or a γ for the charged) (figure 1); the production cross section is a function of the sfermion mass. In the case of the third generation, the mixing angle enters in the production cross section as well. The $\tilde{\nu}_e$ ($\tilde{e}$) can also be produced via the exchange of a chargino (neutralino) in the t-channel, and then the cross section depends on the $\tilde{\chi}^{\pm}$ ($\tilde{\chi}^0$) mass too. The cross sections for sfermions at $\sqrt{s} = 183$ GeV vary typically from 0.1 to 2 pb.

1.3 Direct and indirect decays of gauginos and sfermions

The decay of the produced sparticles can be either direct or indirect. In a *direct decay* the sparticle decays directly or via a virtual exchange to standard particles through an $\not{R}_p$ vertex. An example of the direct decay of a chargino or a neutralino is given in the first diagram of fig. 2.

In an *indirect decay* the sparticle first decays through an R_p-conserving vertex to a standard and on-shell sparticle which then decays through an $\not{R}_p$ vertex. Exemples of charginos and sfermions indirect decay are shown in the second and third diagram of fig. 2) respectively. This indirect decay is the most important in our different analyses not only because it is dominant compared with direct decay but also because it is the unique possible decay of selectron and smuon via $\not{R}_p$couplings.

direct decay	$\tilde{q} \rightarrow q_1\ q_2$ $\tilde{\chi}_1^0 \rightarrow q_1\ \tilde{q} \rightarrow q_1\ q_2 q_3$ $\tilde{\chi}^{\pm} \rightarrow q_1\ \tilde{q} \rightarrow q_1\ q_2 q_3$
indirect decay	$\tilde{\chi}^{\pm} \rightarrow W^{*+}\ \tilde{\chi}_1^0 \rightarrow q_1 q_2\ q_3 q_4 q_5\ q_1 q_2$ *or* $l^+\nu\ q_3 q_4 q_5$ $\tilde{q} \rightarrow q_1\ \tilde{\chi}_1^0 \rightarrow q_1\ q_2 q_3 q_4$ $\tilde{e} \rightarrow e\ \ \tilde{\chi}_1^0 \rightarrow e\ q_1 q_2 q_3$ $\tilde{\mu} \rightarrow \mu\ \tilde{\chi}_1^0 \rightarrow \mu\ q_1 q_2 q_3$ $\tilde{\tau} \rightarrow \tau\ \tilde{\chi}_1^0 \rightarrow \tau\ q_1 q_2 q_3$ $\tilde{\nu} \rightarrow \nu\ \ \tilde{\chi}_1^0 \rightarrow \nu\ q_1 q_2 q_3$

Table 1: Neutralino chargino and sfermion possible decay via $\bar{U}\bar{D}\bar{D}$ coupling is dominant. The indirect decay of stau and sneutrino are not considered in this analysis.

Table 1 showes the different possible direct or indirect decays via $\bar{U}\bar{D}\bar{D}$ couplings of supersymetric particles. The most important features of these direct and indirect decay via $\bar{U}\bar{D}\bar{D}$ couplings is the number of quarks in final state which goes up to 5 for chargino indirect decay. It is worth noticing here that missing energy comes mainly from the neutrino final state in the leptonic decay of the W^*, except the special case of sneutrino indirect decay.

1.4 $\bar{U}\bar{D}\bar{D}$ Couplings.

The $\bar{U}\bar{D}\bar{D}$ Yukawa couplings strength corresponding to squark decay into two quarks can be bound with from above (indirect limits) and below (sensitivity of this analysis).

Upper limits on $\bar{U}\bar{D}\bar{D}$ couplings come from Standard Model constraints with experimental mesurements.

In more details, they come from

- heavy nucleon decays for λ''_{112} couplings [6])
- $n - \bar{n}$ oscilations for λ''_{113} [7])
- $R_l = \Gamma_{had}(Z^0)/\Gamma_l(Z^0)$ for $\lambda''_{312}, \lambda''_{313}, \lambda''_{323}$ [8, 9]).

The other upper limits do not come from experimental bounds. They are obtained from the requirement of perturbative unification at GUT scale of 10^{16} GeV. This gives a limit of 1.25 for a sfermion mass of 100 GeV [10, 6]. Upper limits on the $\bar{U}\bar{D}\bar{D}$ couplings are reported in table 2 [13].

ijk	$\lambda''_{ijk} \leq$	ijk	$\lambda''_{ijk} \leq$	ijk	$\lambda''_{ijk} \leq$
$\lambda''_{uds}(112)$	10^{-6}	$\lambda''_{cds}(212)$	1.25	$\lambda''_{tds}(312)$	0.43
$\lambda''_{udb}(113)$	10^{-5}	$\lambda''_{cdb}(213)$	1.25	$\lambda''_{tdb}(313)$	0.43
$\lambda''_{usb}(123)$	1.25	$\lambda''_{csb}(223)$	1.25	$\lambda''_{tsb}(323)$	0.43

Table 2: Limits [13] on the $\bar{U}\bar{D}\bar{D}$ Yukawa couplings in units of $(m_{\tilde{f}}/100$ GeV), where $m_{\tilde{f}}$ is the appropriate sfermion mass.

A lower limit on these couplings comes from the sensitivity of our analysis which does not search long lived sparticles in the detector (displaced vertices). Therefore a limit can be imposed by requiring a short mean decay length L which is given by [11, 12]:

$$L(cm) = 0.1\ (\beta\gamma) \left(\frac{m_{\tilde{l}}}{100\mathrm{GeV/c^2}}\right)^4 \left(\frac{1\mathrm{GeV/c^2}}{\mathrm{m}_{\widetilde{\chi}}}\right)^5 \frac{1}{\lambda''^2} \tag{3}$$

if neutralino or chargino is the LSP or by

$$L(cm) = 10^{-12}\ (\beta\gamma) \left(\frac{1\mathrm{GeV/c^2}}{\mathrm{m}_{\widetilde{\mathrm{f}}}}\right) \frac{1}{3\lambda''^2} \tag{4}$$

if the sfermion is the LSP. In the two previous formuli $\beta\gamma = P_{\widetilde{\chi},\widetilde{f}}/m_{\widetilde{\chi},\widetilde{f}}$. Our typical lower limit of sensitivity for this analysis ($L \lesssim 1$ cm) is of the order of 10^{-4} (10^{-3}) in case of 30 GeV (10 GeV) $\widetilde{\chi}^0$or $\widetilde{\chi}^{\pm}$mass with sfermion mass of 100 GeV, and 10^{-7} in case of sfermions.

Note that in these analyses the coupling $\lambda''_{212} = 0.5$ is used for signal generation and for MSSM interpration of the results. Then, no assumption on the quark flavour has been made. Searches of λ'' couplings which lead to the production of one or several b quarks, have the advantage of using b-tagging techniques and have better sensitivity. Therefore we can safely assume that our results obtained for the λ''_{212} are valid for the 8 other λ''_{ijk} couplings as well.

1.5 Topologies and analysis strategy

This article will describe the analysis in search of $\widetilde{\chi}_1^0$, $\widetilde{\chi}_1^+$, $\widetilde{q}$, $\widetilde{e}$ and $\widetilde{\mu}$pair produced. The analysis of the different decay channels can be organized on the basis of the number of hadronic jets in the final state. Table 3 displays the different event topologies from direct and indirect decays of different sparticles through $\bar{U}\bar{D}\bar{D}$ couplings.

final states	direct decay of	indirect decay of
$4j$	$\widetilde{q}\widetilde{q}$	
$6j$	$\widetilde{\chi}_1^0\widetilde{\chi}_1^0$, $\widetilde{\chi}_2^0\widetilde{\chi}_1^0$, $\widetilde{\chi}_1^+\widetilde{\chi}_1^-$	
$8j$		$\widetilde{\chi}_2^0\widetilde{\chi}_1^0$, $\widetilde{q}\widetilde{q}$
$10j$		$\widetilde{\chi}_1^+\widetilde{\chi}_1^-$
$6j+\not{E}$		$\widetilde{\chi}_2^0\widetilde{\chi}_1^0$, $\widetilde{\nu}\widetilde{\nu}$
$6j+2l$		$\widetilde{\chi}_2^0\widetilde{\chi}_1^0$, $\widetilde{l}\widetilde{l}$
$6j+2l+\not{E}$		$\widetilde{\chi}_1^+\widetilde{\chi}_1^-$
$8j+1l+\not{E}$		$\widetilde{\chi}_1^+\widetilde{\chi}_1^-$

Table 3: Final states in neutralino chargino and sfermion pair production when the decay via $\bar{U}\bar{D}\bar{D}$ coupling is dominant.

It has been mentioned previously that no missing energy is the principal feature of these final states. Therefore reconstruct masses of the supersymmetric particles becomes possible in all channels. The mass reconstruction of multijet (more than 4 jets) events requires specific methods and tools. Table 4 summarizes specific techniques used for these multijets analyses.

In this section the general features of the mass reconstruction procedure, common to all the analysis channels, will be presented. Channel specific features of the analysis (e.g. selection cuts and neural network configurations) are treated in the chapter of respective decay channel.

- **Clustering**
  The clustering of hadronic jets was performed by the *ckern* package[18] based on the Cambridge clustering algorithm[19]. The choice of this clustering algorithm is motivated by its good performance for configurations with a mixture of soft and hard jets, the expected case for λ'' events. Moreover, the "soft freezing" mechanism of the algorithm provides a good resolution for the jet substructure which is present in $\bar{U}\bar{D}\bar{D}$ indirect decays. For each event *ckern* provides all possible configurations

	$\widetilde{\chi}_1^+\widetilde{\chi}_1^-$		$\widetilde{\chi}_1^0\widetilde{\chi}_1^0$	$\widetilde{q}\widetilde{q}$		$\widetilde{e}\widetilde{e}$	$\widetilde{\mu}\widetilde{\mu}$
decay type	dir	ind	dir	dir	ind	ind	ind
final states	6j	10j	6j	4j	8j	6j+2e	6j+2 μ
Reconstructed mass	$\widetilde{\chi}_1^+$	$\widetilde{\chi}_1^+$ $\widetilde{\chi}_1^0$	$\widetilde{\chi}_1^0$	$\widetilde{q}$	$\widetilde{q}$ $\widetilde{\chi}_1^0$	$\widetilde{e}$ $\widetilde{\chi}_1^0$	$\widetilde{\mu}$ $\widetilde{\chi}_1^0$
NNW pairing method	yes	yes	yes	no	yes	yes	yes
Constraint number in the fit	5	6	5	5	6	6	6

Table 4: List of techniques used in each analysis depanding if the sfermion or chargino decay is direct or not. When the number of jets is greater than 4 a Neural NetWork (NNW) pairing technique is used in order to perform a kinematical rescaling on jets to obtain sparticle masses.

between two and ten jets. The resulting values of the variables $y_{(i+1)i}$, the transition values of the DURHAM resolution variable, y_{cut}, which change the event from an i to an i+1 jet configuration, constitutes a powerful tool for identifying the topologies in the multijet signals. By applying a cut, y_{cut}, on the variable $y_{(i+1)i}$, the event is demanded to have at least an (i+1)-jet configuration. For reasons of convenience, the cut is rather applied on the negative logarithm of $y_{(i+1)i}$ than on the value itself.

- **Jet pairing**
  The jets pairing, the association of each jet with its parent sparticle, was for each analysis performed by a neural network. The SNNS [20] package was used for the construction and training of the neural networks. The exact configuration of input and hidden nodes of the networks depends on the specific analysis channel, whereas each output node represents a jet in the final state. The training was performed in a standard backpropagation manner, on samples of 20.000 patterns from a toy Monte Carlo generator, with only decay and boost implemented at the quark level, and the performance validated on a seperate set of similar patterns. The indirect sfermion and chargino analysis was divided into four windows in the sfermion-neutralino mass plane. Due to the large variations in event shapes the neural networks were also trained separately for each window.

- **Kinematical rescaling**
  All topologies considered in this paper give us the possibility to reconstruct masses with 5 or 6 constraints depending on wheter the two neutralinos are decay products of the first sparticle pair produced, i. e. indirectly. The rescaling algorithm, based on W^+W^-multijets mass reconstruction algorithm [21] uses the Lagrange multiplier method. The constraint imposed to rescal jets momenta are energy and momentum conservation and equal mass. The second mass constraint is imposed on a given number of jets which come from the 2 neutralinos in the cascade decay. For example, consider a pair of squarks (a and b) which decay indirectely throught the neutralino (c and d respectively) in 2N jets (N jets each). Therefore, the secondary decay of the neutralino can give a mass resonance with 3 jets among the N squark jets. In

this case the two mass constraints can be written after the pairing method :

$(\sum P_a(i), i = 1, N)^2 = (\sum P_b(i) = i = N + 1, 2N)^2$

and

$(\sum P_c(i), i = 1, 3)^2 = (\sum P_d(i), i = N + 1, N + 3)^2$

where i is the jet number.

2 Data and MC samples

The data corresponding to an integrated luminosity of 53. pb^{-1} collected during 1997 by the DELPHI detector [14] at center of mass energies around 183 GeV were analysed.

Concerning the background, the different contributions coming from the Standard Model processes: $e^+e^- \rightarrow Z\gamma$, W^+W^-, ZZ were considered. For the study of four fermion final states, the PYTHIA [15] generator was used; a cross check was performed using the four-fermion final states generated with EXCALIBUR [16].

To evaluate signal efficiencies, sparticle production was generated using SUSYGEN [17]. All generated signal events were processed with the DELPHI detector simulation program. List of generated points are given in the section corresponding to each channel.

3 Analyses

3.1 Hadronic Preselection

In order to reject non hadronic standard model background the following preselection criteria were applied for all the analyses reported below:

- the charged multiplicity has to be greater or equal to 14;
- the total event energy was required to be greater than $0.30 \times \sqrt{s}$;
- the total energy from neutral particles was required to be less than $0.50 \times \sqrt{s}$.

With this preselection most of the $\gamma\gamma$ background is supressed. Higher charged multiplicity cuts included in each analysis make this background irrelevant for this hight jet multiplicity analyses with no missing energy.

3.2 Charginos and neutralinos, 10 and 6 jet analyses

3.2.1 Direct decay of $\widetilde{\chi}_1^0\widetilde{\chi}_1^0$ or $\widetilde{\chi}_1^+\widetilde{\chi}_1^-$ in 6 jets

Signal events are selected with sequential cuts given in table 10. To apply these cuts we have considered three different mass windows corresponding to different main backgrounds. In the first analysis mass window ($5 \leq m_{\tilde{\chi}} \leq 30$) the 6 jet signal is more similar to a 2 jet event than a 4 jet W^+W^-event. Then in this first case the main background is the QCD ($Z\gamma$) one. The main backround of the third analysis mass window ($60 \leq m_{\tilde{\chi}} \leq 92$) corresponding to high neutralino or chargino masses is mainly composed with W^+W^-events. This can be easly understood from the fact that no 4 jet W mass reconstruction cut can be apply for this mass range of signal. The background of the intermediate analysis mass window is composed with both W^+W^-, ZZ and QCD ($Z\gamma$) events.

The first 9 cut variables of table 10 are applied against initial state radiation when the emmitted photon is detected or lost in the beam pipe. The reconstructed mass cut in 4 jet variable is important for the two first windows to supress most of the W^+W^-events. Cut variables 11 to 15 such as y_{43}, y_{54} and y_{65} correspond to hight jet multiplicity event selection. Figure 3 shows two examples of these cuts.

The last selection used the six jet mass reconstruction method presented in the introduction. The neural network pairing method used 6 output nodes corresponding to each jet. For the training of the network 3 nodes corresponding to the same neutralinos are set to 1 and the 3 other nodes are set to 0. the input nodes of the network are the 15 di-jet masses obtained after a 4 comstraint rescaling.

A energy-momentum conservation and equal masse constraints are used to rescale the energy-momentum of each of the jets. The resolution of the six jet mass reconstruction is around 6 GeV and becomes higher for the highest masses. An example of such mass reconstruction for the signal, data and MC background is plotted in figure 5 for a neutralino mass of 69 GeV which corresponds to the third analysis window.

After signal selection no excess in Data compared to expected Monte-Carlo Standard Model backround had been found. Final event numbers are summarized in table 5. Signal efficiency obtained from the different simulated points are reported and the number of

signal events excluded with a 95 % of Confidential Level (CL), N^{95} and the corresponding excluded cross section σ^{95} are given in the same table.

6 jet analysis : results and efficiency						
Mass range (GeV)	$5 \leq m_{\tilde{\chi}} \leq 30$		$30 \leq m_{\tilde{\chi}} \leq 60$		$60 \leq m_{\tilde{\chi}} \leq 92$	
Mass point in GeV	15	22	38	52	68	80
ϵ (%)	17	23	22	28	29	16
SM	4.8	12.8	2.3	10.	21.2	46.2
Data	2	17	5	9	18	46
N^{95}	4.24	13.25	8.48	7.4	9.	15.37
σ^{95} (pb)	0.47	1.08	0.68	0.50	0.58	1.80

Table 5: Signal efficiency, remaining data, expected SM background (W^+W^-, $Z\gamma$ and ZZ) for each mass window of the 6 jet analysis. The corresponding N^{95} and σ^{95} are also reported

3.2.2 Indirect decay of $\widetilde{\chi}_1^+\widetilde{\chi}_1^-$ in 10 jets

The 10 jet signal topology is more or less equivalent to the previous one. The main difference comes from the indirect decay of chargino with different possible mass combination between a chargino and a neutralino which gives different jet topologies.

We separate this analysis in 4 different windows, which correspond to two chargino mass ranges and two neutralino mass ranges. Signal selection for these 4 window analyses take into account mainly the different jet topologies coming from different kinematics due to the difference of mass between chargino and neutralino.

Table 11 gives cut variable values of each mass analysis window. Cut variables 1 to 9 have already been used for the six jet analysis. Different y_{ij} variables have been used up to 10 jet configuration. Example of these cuts are shown in figure 5.

Mass reconstruction of charginos and **neutralino** using the NNW pairing method has also been used. The 10 output nodes of the neural network correspond to the 10 jet and set of values (1.,1.,1.,.75,.75,0.25,0.25,0.,0.,0.) for the training has been presented to the network. Input nodes of the network are the 45 di-jet masses. The resolution of the neutralino is not very good for all mass differences and cannot be used to select the signal with a good efficiency. However it does not mean that this neutralino mass reconstruction is a nonesense. Indeed, to find the neutralino and chargino masses we have applied a 6 constraint rescaling with 2 equal mass constraints (for the 2 neutralinos and for the 2 charginos). Then the resolution on the chargino mass is better than a standard 5 constraint rescaling in 10 jets. The mass resolution depends a lot on the mass difference between chargino and neutralino. As an example resolution of 10 GeV for charginos around 70 GeV and neutralinos around 50 GeV is obtained. Reconstructed mass plots are shown in figure 5. note that the signal over backround ratio is good enough for a signal produced with 1 pb cross section. For the last selection, we ask the reconstructed chargino mass appear in the mass analysis window.

No excess was found in Data compared with excpected background in each analysis window. Table 6 summarize Data and Monte-Carlo event numbers and signal efficencies for the genereted points. The corresponding N^{95} and σ^{95} are also presented in the same table. Notice that the number of expected events is higher in the fourth mass window due to the W^+W^-background.

$\widetilde{\chi}_1^+\widetilde{\chi}_1^-$10 jet analysis : results														
Mass range (GeV)	$45 \leq m_{\tilde{\chi}} \leq 70$								$70 \leq m_{\tilde{\chi}} \leq 92$					
Mass range (GeV)	$5 \leq m_{\tilde{\chi}_1^0} \leq 35$				$35 \leq m_{\tilde{\chi}_1^0} \leq 70$				$5 \leq m_{\tilde{\chi}_1^0} \leq 45$			$45 \leq m_{\tilde{\chi}_1^0} \leq 92$		
$m_{\tilde{\chi}_1^+}$	52	48	68	68	52	69	69	68	71	71	82	82	82	82
$m_{\tilde{\chi}_1^0}$	10	22	10	22	48	38	52	64	10	22	22	49	68	78
ϵ %	16	19	19	26	19	29	29	15	14	26	32	52	32	5
SM	5.7				3.2				10.7			11.4		
DATA	3				3				10			11		
N^{95}	4.77				5.29				7.95			8.48		
$\sigma^{95}(pb)$	0.08				0.09				0.15			0.16		

Table 6: Signal efficency, remaining data, expected SM background (W^+W^-, $Z\gamma$ and ZZ) for each mass window of the 10 jet analysis. The corresponding N^{95} and σ^{95} are also reported.

3.3 Squark analysis

Squark searches in the case of a dominant R-parity violating $\bar{U}\bar{D}\bar{D}$ coupling were performed in the indirect decay mode. In the direct mode each squark decays through a $\bar{U}\bar{D}\bar{D}$ vertex to two quarks, whereas in the indirect decay channel each squark decays, conserving R-parity, to a quark and a $\widetilde{\chi}_1^0$, which then in turn decays through a $\bar{U}\bar{D}\bar{D}$ coupling to three quarks. The two resulting hadronic event signatures are thus four and eight hadronic jets respectively, without missing energy. The general analysis methods previously described in chapter 1, based on reconstruction of sparticle masses, were adopted for the analysis of indirect squark decays.

3.3.1 Indirect squark analysis

In this analysis, the indirect decay of squarks through a dominant $\bar{U}\bar{D}\bar{D}$ coupling was considered. The analysis was performed for a generic $\bar{U}\bar{D}\bar{D}$ coupling without consideration taken to flavour dependent properties, e.g. b-tagging. The final states in the indirect decay channel contain eight quarks of any flavour, but the topology of the signal strongly depends on the mass of the $\widetilde{\chi}_1^0$, through which the decay proceeds. The plane of possible squark and neutralino masses was therefore divided into four separate analyses and SUSY signals were simulated at different squark masses in the range 55-85 GeV with $\widetilde{\chi}_1^0$masses between 10-80 GeV. For each analysis, a neural network was trained for the pairing of 8 jets. The 56 trijet mass combinations from the 8 jet event topologies, after the Cambridge clustering [18], were used as input to the neural network. A mass reconstruction was thereafter performed with a 6 constraints (energy, momenta and masses) kinematical fit, resulting in reconstructed masses of both squark and neutralino. The efficiency of the mass reconstruction for simulated signals was better than 80% and the resolution in reconstructed squark masses better than $\pm$10 GeV. The resolution in reconstructed neutralino masses showed large variations depending on generated neutralino mass, but was better than $\pm$10 GeV for $m_{\tilde{q}} - m_{\widetilde{\chi}_1^0} \leq 40$ GeV.

The 8 jet analysis was aimed at a good sensitivity for R-parity violating $\bar{U}\bar{D}\bar{D}$ signals all over the plane of kinematically available squark and $\widetilde{\chi}_1^0$masses. In addition to a successful mass reconstruction various selection criteria were applied in order to discriminate a signal from standard model backgrounds from $Z\gamma$, W^+W^- and ZZ events. A general event selection was made for all four analysis windows with the aim of a maximum general signal efficiency and a good rejection of low multiplicity hadronic events. Thereafter, a few specific cuts were independently tuned for each analysis window. The selection cuts are presented in table 12 and are illustrated together with the mass reconstruction in fig.7.

The agreement between data and standard model backgrounds is good at all levels of the analysis and no evidence of an R-parity violating $\bar{U}\bar{D}\bar{D}$ signal has been detected. The final numbers are in agreement with the expected background in all four analysis windows. The efficiency was calculated at each of the generated points and interpolated in the regions between. Efficiencies for the signal after cuts range from 26-34%, for small or large mass differences between squark and neutralino, up to 72% for the most easily distinguished mass combination. In the case of degenerate masses (a mass difference between squark and neutralino of less than 5 GeV) the event topology closely resembles a 6 jet event and is hence not treated by this analysis. Final numbers of selected events

$\widetilde{q}\widetilde{q}$ 8 jet analysis: results																
Mass range (GeV)	$45 \leq m_{\tilde{q}} \leq 70$							$70 \leq m_{\tilde{q}} \leq 92$								
Mass range (GeV)	$5 \leq m_{\tilde{\chi}_1^0} \leq 35$				$35 \leq m_{\tilde{\chi}_1^0} \leq 70$			$5 \leq m_{\tilde{\chi}_1^0} \leq 45$				$45 \leq m_{\tilde{\chi}_1^0} \leq 92$				
$m_{\tilde{q}}(GeV)$	55		65		55		65	75		85		75		85		
$m_{\tilde{\chi}_1^0}$ (GeV)	10	30	10	30	50	40	60	10	30	10	30	50	70	60	80	
ϵ (%)	26	63	29	68	31	67	33	34	72	32	72	68	33	72	30	
SM	100.2				74.4			115.1				58.9				
Data	99				71			111				57				
N_{95}	20.7				16.4			20.1				15.9				
$\sigma_{95}(pb)$	0.39				0.31			0.38				0.30				

Table 7: Generated masses and efficiencies of the signals together with final numbers of data and Standard Model backgrounds. The table also shows the maximum number of signal events and cross section at 95% confidence level in each analysis window.

from data and background can be found in table 7 together with the efficiencies for each of the generated signals.

3.4 Selectrons and smuons analysis

With a $\bar{U}\bar{D}\bar{D}$ dominant coupling the only possible decay for selectrons smuons and sneutrinos is indirect (see figure 2).

3.4.1 Selectrons indirect decay into $6j+e^+e^-$

Final state of selectrons pair indirect decay are easy to identify. These events have a high hadronic activity (6 jets) with one e^- and one e^+. Therefore this analysis is very sensitive to a good identification and mesurement of the most energetic electron and positron. In this analysis e^- and e^+ are tagged loose and isolated to keep high efficiency. Isolation criterion is energy less than 10 GeV in a cone of 15 degrees around the tagged leptons. In this analysis we used the same mass windows already used for charginos and indirect squarks.

In table 13 we give all cut values for each analysis window. Two examples of specific cuts for this analysis are shown in figure 10. The main cut is the minimum energy of the tagged electron and positron $E_{e^\pm}^{tag}$. A clusterisation of the hadronic part of the event has been performed to cut in the jet resolution variable i.e. y_{43}^{had} and y_{54}^{had}. Cuts 1 to 7 are the standard variables against the radiative return on the Z. Cuts 8 to 10 are topological cuts against W^+W^-events. Mass reconstruction is possible in this type of final states. Therefore, a specific method developed where we use the information on the two tagged leptons. Then the rescaling is performed with 6 constraints (2 equal mass constraints : $M\widetilde{e}$(1 e + 3 j)=$M\widetilde{e}$(1 e + 3j) and $M\widetilde{\chi}_1^0$(3 j)=$M\widetilde{\chi}_1^0$(3 j)). The pairing is performed with 6 output nodes corresponding to the 6 jets (1,1,1,0,0,0). An example on the selectron and neutralino reconstructed masses is shown in figure 5. Mass information in this analysis is not necessary to selected the signal from the background since the lepton energy cut is sufficient. But in case of Data excess we are able to see a nice resonance in selectron mass. The mass resolution is very sensitive to detector reconstruction electron momentum.

No significant excess of Data have been found. In table 8 we sum up all numbers for Data and expected Standard Model events. Signal efficencies are also reported for all simulated points.

3.4.2 Smuons indirect decay into $6j + \mu^+\mu^-$

This analysis is equivalent to the previous one replacing electron by muon in ther final state. Therefore the main difference of this analysis comes from the better identification and energy reconstruction of the muon than the electron one. List of cuts is given in table 14. These variables are the same as selectron analysis. Example of specific cuts for this analysis is shown in figure 10. The better detection efficency and mesurement of muons allow us to reconstruct smuon mass with a very good resolution as can be seen in figure 5. In this case also, an excess of Data can produce a resonance in the mass plot. Nevertheless, no excess have been found in this analysis, and final numbers of events and signal efficencies are given in table 9.

Selectrons 6j + e^+ e^- analysis : Results																
Mass range (GeV)	$45 \leq m_{\tilde{e}} \leq 70$							$70 \leq m_{\tilde{e}} \leq 92$								
Mass range (GeV)	$5 \leq m_{\tilde{\chi}_1^0} \leq 35$				$35 \leq m_{\tilde{\chi}_1^0} \leq 70$			$5 \leq m_{\tilde{\chi}_1^0} \leq 45$				$45 \leq m_{\tilde{\chi}_1^0} \leq 92$				
$m_{\tilde{e}}(GeV)$	55		65		55		65	75		85		75		85		
$m_{\tilde{\chi}_1^0}$ (GeV)	10	30	10	30	50	40	60	10	30	10	30	50	70	60	80	
ϵ (%)	16	30	28	33	15	30	20	26	32	34	35	33	19	37	22	
SM	2.53				3.90			0.39				3.46				
Data	2				1			0				3				
N^{95}	4.69				3.71			3.17				5.29				
$\sigma^{95}(pb)$	0.09				0.07			0.06				0.09				

Table 8: Signal efficiencies, remaining data, expected SM background (W^+W^-, $Z\gamma$ and ZZ) for each mass window of the selectrons analysis. The corresponding N^{95} and σ^{95} is also reported.

Smuons 6j + μ^+ μ^- analysis : Results																
Mass range (GeV)	$45 \leq m_{\tilde{e}} \leq 70$							$70 \leq m_{\tilde{e}} \leq 92$								
Mass range (GeV)	$5 \leq m_{\tilde{\chi}_1^0} \leq 35$				$35 \leq m_{\tilde{\chi}_1^0} \leq 70$			$5 \leq m_{\tilde{\chi}_1^0} \leq 45$				$45 \leq m_{\tilde{\chi}_1^0} \leq 92$				
$m_{\tilde{\mu}}(GeV)$	55		65		55		65	75		85		75		85		
$m_{\tilde{\chi}_1^0}$ (GeV)	10	30	10	30	50	40	60	10	30	10	30	50	70	60	80	
ϵ (%)	28	45	25	60	31	55	39	26	49	28	48	39	22	42	22	
SM	0.51				0.62			0.39				0.25				
Data	1				0			1				0				
N^{95}	4.76				3.17			4.76				3.18				
$\sigma^{95}(pb)$	0.08				0.06			0.08				0.06				

Table 9: Signal efficiencies, remaining data numbers and expected SM background (W^+W^-, $Z\gamma$ and ZZ) for each mass window of the smuons analysis. The corresponding N^{95} and σ^{95} is also reported.

4 MSSM interpretation of Results

In each chanel of this analysis no excess has been seen in data with respect to the expected SM background. Therefore limits at 95 % of confidence level on the cross section of each processes can be obtained. Then mass limit can be derived for supersymmetric particles.

4.1 Chargino and neutralino multijet searches

Combining the 6-jet analysis (used for the direct decay of $\tilde{\chi}_1^+\tilde{\chi}_1^-$ or $\tilde{\chi}_1^0\tilde{\chi}_1^0$) and the 10-jet analysis (used for indirect decay of $\tilde{\chi}_1^+\tilde{\chi}_1^-$) results, an exclusion contour in μ, M_2 plane at 95 % confidence level has been derived for different values of m_0 (90 and 300 GeV/c^2) and tanβ (1.5 and 90). These exclusion contour plot in μ, M_2 plane are shown in figure 12.

The experimental cross section (σ^{95}) that can be excluded at 95 % confidence level, is obtained from Data and Monte-Carlo numbers given in tables 5 and 6. Signal efficency for any value of μ, M_2 (i.e $\tilde{\chi}_1^0$and $\tilde{\chi}^{\pm}$masses) is interpolated using efficency grid of the full Delphi detector simulation given in the same tables. A μ, M_2 point of the plane is excluded at 95 % confidence level if the signal cross section time the efficency of the signal at this point is greater than experimental cross section (σ^{95})

4.2 Indirect squark multijet searches

Exclusion domains in the squark-neutralino mass plane is obtained by calculating N_{95} divided by the integrated luminosity times the efficiency for each 1×1 GeV bin and comparing to the cross section for pair-produced squarks. The resulting exclusion contours for stop and sbottom squarks can be seen in fig.13. A 100% branching ratio of indirect decays in the neutralino channel is assumed for this exclusion. The performed 8 jet analysis is independent of squark flavour and hence the difference in exclusion between different squarks is only manifested through their different production cross section. The exclusion contours of stop and sbottom squarks respectively is therefore, more generally, also valid for other squark generations.

By combining these results with the constraint on the neutralino mass ($m_{\tilde{\chi}_1^0} > 21$ GeV) from the gaugino searches, lower bounds on the squark masses are achieved.

- $m_{\tilde{t_1}} \geq 62.5$ GeV, for $\Phi_{mix} = 0$ rad
- $m_{\tilde{t_1}} \geq 49$ GeV for $\Phi_{mix} = 0.98$ rad
- $m_{\tilde{b_1}} \geq 58.5$ GeV, for $\Phi_{mix} = 0$ rad

4.3 Indirect selectron and smuon multijet searches

Exclusion limit in the $\tilde{\chi}_1^0$and $\tilde{e}(\tilde{\mu})$ mass plane are obtained from results of tables 8 and 9. The excluded cross section at 95 % of confidence level are compared with the effective (taking into account signal efficency) signal cross section. Results for (left and right) selectrons and smuons are shown in figure 14 and 15. Value of tanβ = 1.5 and μ = -200 GeV have been used in the scan. For mass difference between sleptons and neutralino greater than 5 GeV we can excluded a right and left selectron mass :

- $m_{\tilde{e_R}} \geq 70$ GeV and $m_{\tilde{e_L}} \geq 53$ GeV

and right and left smuon mass of

- $m_{\tilde{\mu_R}} \geq 68$ GeV and $m_{\tilde{\mu_L}} \geq 69$ GeV

5 Conclusion

Searches for $\not{R}_p$ effects in e^+e^- collisions at $\sqrt{s} = 183$ GeV have been performed with the DELPHI detector. The pair production of neutralinos, charginos,squarks selectrons and smuons has been studied with a dominant $\bar{U}\bar{D}\bar{D}$ R-parity violating coupling. No evidence for R-parity violation has been observed so far, therefore limits have been set within the MSSM framework, as summarized below.

The study of direct and indirect decays of neutralinos and charginos via a $\bar{U}\bar{D}\bar{D}$ coupling allowed to constrain the MSSM parameter space extending the region excluded by LEP1. With $m_0 = 150$ GeV and $tan\beta = 1$. a limit on :

- Neutralinos mass : $m_{\tilde{\chi}_1^0} \geq 21$ GeV
- Charginos mass : $m_{\tilde{\chi}_1^+} \geq 87$ GeV

The indirect decay squark searches allowed to constrain stop and sbottom masses :

- $m_{\tilde{t_1}} \geq 62.5$ GeV, for $\Phi_{mix} = 0$ rad
- $m_{\tilde{t_1}} \geq 49$ GeV, for $\Phi_{mix} = 0.98$ rad
- $m_{\tilde{b_1}} \geq 58.5$ GeV, for $\Phi_{mix} = 0$ rad

for $\Delta M \geq 5$ GeV.

The indirect decay selectrons and smuons searches allowed to constrain selectrons and smuons masses: Smuons mass limit for $\Delta M \geq 5$ GeV and for $\tilde{\chi}_1^0 \geq 21$ GeV

- $m_{\tilde{\mu_R}} \geq 68$ GeV
- $m_{\tilde{\mu_L}} \geq 69$ GeV
- $m_{\tilde{e_R}} \geq 70$ GeV
- $m_{\tilde{e_L}} \geq 53$ GeV

Acknowledgements

We are greatly indebted to our technical collaborators and to the funding agencies for their support in building and operating DELPHI detector. We are particularly thankful to the members of the CERN-SL Division for the excellent performance of LEP during the high energy run of 1997. The financial support of STINT, The Swedish Foundation for International Cooperation in Research and Higher Education, and NFR, The Swedish Natural Science Research Council, is highly appreciated.

References

[1] For reviews, see e.g. H.P. Nilles, *Phys. Rep.***110** (1984) 1; H.E. Haber and G.L. Kane, *Phys. Rep.* **117** (1985) 75.

[2] P. Fayet, *Phys. Lett.* **B69** (1977) 489; G. Farrar and P. Fayet, *Phys. Lett.* **B76** (1978) 575.

[3] S. Weinberg, *Phys. Rev.* **D26** (1982) 287.

[4] I. Hinchliffe and T. Kaeding, *Phys. Rev.* **D47** (1993) 279.

[5] C.E. Carlson et al., *Phys. Lett.* **B357** (1995) 99.

[6] J.L. Goity, Marc Sher, Phys. Lett. B 346 (1995) 69, erratum-ibid. B 385 (1996) 500, hep-ph/9412208.

[7] F. Zwirner, Phys. Lett. B 132 (1983) 103.

[8] G. Bhattacharyya, J. Ellis, K. Sridhar, Mod. Phys. Lett. A10 (1995) 1583, hep-ph/9503264; G. Bhattacharyya, D. Choudhury, K. Sridhar, Phys. Lett. B 355 (1995) 193, hep-ph/9504314; J. Ellis, S. Lola, K. Sridhar, e-Print Archive: hep-ph/9705416.

[9] G. Bhattacharyya, Nucl. Phys. Proc. Suppl. 52A (1997) 83, hep-ph/9608415.

[10] B. Brahmachari, Probir Roy, Phys. Rev. D 50 (1994) 39, erratum-ibid. D 51 (1995) 3974, hep-ph/9403350.

[11] S. Dawson, *Nucl. Phys.* **B261** (1985) 297.

[12] H. Dreiner and G.G. Ross, *Nucl. Phys.* **B365** (1991) 597.

[13] H. Dreiner, hep-ph/9707435.

[14] P. Abreu et al., *Nucl. Instr. Meth.* **378** (1996) 57.

[15] T. Sjöstrand, *Computer Phys. Comm.* **39** (1986) 347.

[16] F.A. Berends, R. Kleiss, R. Pittau, *Computer Phys. Comm.* **85** (1995) 437.

[17] S. Katsanevas, P. Morawitz, hep-ph/9711417, sumbitted to Comp. Phys. Comm.

[18] S. Bentvelsen and I. Meyer, hep-ph/9803322, submitted to *Eur. Phys. J.***C**. The *ckern* package can be found on wwcn1.cern.ch/˜ stamb/ckern/ckern.html

[19] Yu.L. Dokshitzer, G.D. Leder, S. Moretti, B.R. Webber *J. High Energy Phys.***08** (1997) 001.

[20] Stuttgart Neural Network Simulator User manual, version 4.1 http://www-ra.informatik.uni-tuebingen.de/SNNS/

[21] A. Duperrin, A multijet rescaling alghorithm DELPHI DELPHI 97-170 PHYS 745.

6 jet analysis : Cuts				
	Mass range (GeV)	$5 \leq m_{\tilde{\chi}} \leq 30$	$30 \leq m_{\tilde{\chi}} \leq 60$	$60 \leq m_{\tilde{\chi}} \leq 92$
1	$E_{neutral} \leq$	45 GeV	60 GeV	60 GeV
2	$E_{charged} \geq$	60 GeV	60 GeV	60 GeV
3	$n_{charged} \geq$	25	25	25
4	$n_{total} \geq$	15	15	15
5	$E^i_{em} / E^i (i = 1, 3) \leq$	.9	.9	.9
6	$n^i_{charged} (i = 1, 3) \geq$	2	2	2
7	$E^{max}_{\gamma} \leq$	20 GeV	20 GeV	20 GeV
8	$P_{miss} \leq$	45 GeV	45 GeV	45 GeV
9	$\sqrt{s'} \geq$	160 GeV	160 GeV	160 GeV
10	$M^{5C}_{4j} \in$	[0.,50.]GeV	[25,70] GeV	[50.,92.] GeV
11	$-log(y_{43}) \in$	[4.5,7.5]	[2.5,5.]	[1.,4.5]
12	$\alpha^5 E^5_{min} \geq$	1.2 rad.GeV	1.5 rad.GeV	6. rad.GeV
13	$\alpha^5 E^5 \geq a * \beta^5 E^5_{max} / E^5_{min} + b$	1.8,1.8/4.	4.,1./2.	7., 7./9.
14	$-log(y_{54}) \in$	[6.,8.5]	[3.,6.]	[2.,5.]
15	$-log(y_{65}) \in$	[6.,9.5]	[4.,6.5]	-
16	$\lvert M^{5c}_{3j} - M_{\chi} \rvert \leq$	4 GeV	4 GeV	8 GeV

Table 10: List of cuts used in the 6 jets analysis : α^5, β^5 corresponds to the minimum angle between the five jets and the minimum angle between the most energetic jet and the others. E^5_{max} E^5_{min} is the energy corresponding to the most and the least energetic jet. The value y_{ij} corresponds to the durham resolution parameter for a transition from i jets to j jets configuration, (with i=j+1).

$\widetilde{\chi}_1^+\widetilde{\chi}_1^-$ 10 jet analysis : Cuts					
	Mass range (GeV)	$45 \leq m_{\tilde{\chi}} \leq 70$		$70 \leq m_{\tilde{\chi}} \leq 92$	
	Mass range (GeV)	$5 \leq m_{\tilde{\chi}_1^0} \leq 35$	$35 \leq m_{\tilde{\chi}_1^0} \leq 70$	$5 \leq m_{\tilde{\chi}_1^0} \leq 45$	$45 \leq m_{\tilde{\chi}_1^0} \leq 92$
1	$E_{neutral} \leq$	60 GeV	60 GeV	60 GeV	60 GeV
2	$E_{charged} \geq$	60 GeV	60 GeV	60 GeV	60 GeV
3	$n_{neutral} \geq$	10	10	10	10
4	$n_{charged} \geq$	20	20	20	20
5	$E^i_{em}/E^i (i = 1, 3) \leq$	.7	.7	.7	.7
6	$n^i_{charged} (i = 1, 3) \geq$	2	2	2	2
7	$E^{max}_{\gamma} \leq$	20 GeV	20 GeV	20 GeV	20 GeV
8	$P_{miss} \leq$	30 GeV	35 GeV	30 GeV	30 GeV
9	$\sqrt{s'} \geq$	140 GeV	140 GeV	140 GeV	140 GeV
10	$-log(y_{43}) \leq$	5.	5.	5.	5.
11	$M^{5C}_{4jet} \leq$	70 GeV	70 GeV	-	-
12	$\alpha^5 E^5 \geq$	2.5 rad.GeV	4 rad.GeV	5 rad.GeV	6 rad.GeV
13	$-log(y_{54}) \leq$	6	5.5	5	5
14	$-log(y_{65}) \leq$	7.5	6.5	6	6
15	$-log(y_{87}) \leq$	8.5	8.5	7.5	7.5
16	$-log(y_{109}) \leq$	-	-	9	9
17	$M^{6C}_{(5jets)} \in$	[45-70]	[45-70]	[70-92]	[70-92]

Table 11: List of cuts used in the $\widetilde{\chi}_1^+\widetilde{\chi}_1^-$10 jets analysis. The value y_{ij} corresponds to the durham resolution parameter for a flip from i jets to j jets configuration, (with i=j+1). We use in this table the same variable definitions as in the six jet analysis. $M^{6C}_{(5jets)}$ means the reconstructed chargino mass with 10 jets performing a 6 constraints rescaling.

$\widetilde{q}\widetilde{q}$ 8 jet analysis: Cuts					
	Mass range (GeV)	$45 \leq m_{\tilde{q}} \leq 70$		$70 \leq m_{\tilde{q}} \leq 92$	
	Mass range (GeV)	$5 \leq m_{\tilde{\chi}^0_1} \leq 35$	$35 \leq m_{\tilde{\chi}^0_1} \leq 70$	$5 \leq m_{\tilde{\chi}^0_1} \leq 45$	$45 \leq m_{\tilde{\chi}^0_1} \leq 92$
1	$E_{neutral} \leq$	85 GeV	85 GeV	85 GeV	85 GeV
2	$E_{total} \leq$	235 GeV	235 GeV	235 GeV	235 GeV
3	$n_{charged} \geq$	30	30	30	30
4	$E^i_{em}/E^i (i = 1, 3) \leq$	0.56	0.56	0.56	0.56
5	$E^{max}_{\gamma} \leq$	20 GeV	20 GeV	20 GeV	20 GeV
6	$P_{miss} \leq$	95 GeV	95 GeV	95 GeV	95 GeV
7	$Oblatness \leq$	0.52	0.52	0.52	0.52
8	$-log(y_{43}) \leq$	5.4	5.4	5.4	5.4
9	$\alpha^5 E^5 \geq$	3 radGeV	6 radGeV	3 radGeV	7 radGeV
10	$-log(y_{54}) \leq$	6.6	6.6	6.6	6.6
11	$-log(y_{65}) \leq$	8.0	6.7	8.0	6.1
12	$-log(y_{87}) \leq$	8.7	9.5	9.0	9.6

Table 12: Selection criteria in the indirect squark analysis. The first three cuts remove low multiplicity hadronic background, e.g. two-photon events. The following three cuts reduce the ISR background and the last cuts are used to optimise the hadronic selection for the 8 jet signals of each analysis window.

Selectrons 6j + 2e analysis : Cuts					
	Mass range (GeV)	$45 \leq m_{\tilde{e}} \leq 70$		$70 \leq m_{\tilde{e}} \leq 92$	
	Mass range (GeV)	$5 \leq m_{\tilde{\chi}^0_1} \leq 35$	$35 \leq m_{\tilde{\chi}^0_1} \leq 70$	$5 \leq m_{\tilde{\chi}^0_1} \leq 45$	$45 \leq m_{\tilde{\chi}^0_1} \leq 92$
1	$E_{neutral} \geq$	45 GeV	60 GeV	-	50 GeV
2	$E_{charged} \leq$	-	80	-	80 GeV
3	$E^i_{em}/E^i (i = 1, 3) \leq$	.7	.7	.5	.5
4	$n^i_{charged} (i = 1, 3) \geq$	2	2	2	2
5	$E^{max}_{\gamma} \leq$	-	-	-	40
6	$P_{miss} \leq$	30 GeV	35 GeV	30 GeV	30 GeV
7	$\sqrt{s'} \geq$	140 GeV	140 GeV	150 GeV	150 GeV
8	$\alpha^5 E^5 \geq$	-	8 rad.GeV	-	8 rad.GeV
9	$-log(y^{had}_{43}) \geq$	1.5	4.	-	-
10	$-log(y^{had}_{54}) \geq$	-	5.	-	-
11	$E^{tag}_{e^{\pm}} \geq$	6 GeV	4 GeV	15 GeV	3 GeV

Table 13: List of cuts used in the $\widetilde{e}^+\widetilde{e}^-$ analysis. $E^{tag}_{e^{\pm}}$ is the isolated tagged (loose) $e^{\pm}$ energy. Isolation criteria corresponds to a 15 deg. cone around the tagged lepton with energy less than 10 GeV. The value y^{had}_{ij} corresponds to the durham resolution parameter for a flip from i jets to j jets configuration, (with i=j+1) whithout the two tagged leptons.

$6j + \mu^+\mu^-$ analysis : Cuts					
	Mass range (GeV)	$45 \leq m_{\tilde{\mu}} \leq 70$		$70 \leq m_{\tilde{\mu}} \leq 92$	
	Mass range (GeV)	$5 \leq m_{\tilde{\chi}_1^0} \leq 35$	$35 \leq m_{\tilde{\chi}_1^0} \leq 70$	$5 \leq m_{\tilde{\chi}_1^0} \leq 45$	$45 \leq m_{\tilde{\chi}_1^0} \leq 92$
1	$E_{neutral} \geq$	90 GeV	80 GeV	110 GeV	80 GeV
2	$E_{charged} \leq$	55 GeV	75 GeV	35 GeV	50 GeV
3	$E^i_{em}/E^i (i = 1, 2, 3) \leq$	.7	.7	.5	.5
4	$n^i_{charged} (i = 1, 2, 3) \geq$	2	2	2	2
5	$E^{max}_{\gamma} \leq$	-	-	-	40
6	$P_{miss} \leq$	35 GeV	35 GeV	30 GeV	30 GeV
7	$\sqrt{s'} \geq$	130 GeV	140 GeV	150 GeV	150 GeV
8	$\alpha^5 E^5 \geq$	1.5 rad.GeV	5 rad.GeV	-	8 rad.GeV
9	$-log(y^{had}_{43}) \geq$	7.	5.	7	4
10	$-log(y^{had}_{54}) \geq$	7.5	6.	7.5	5
11	$-log(y^{had}_{65}) \geq$	8.	7.	8.	7.5
12	$E^{tag}_{\mu^\pm} \geq$	15 GeV	4 GeV	15 GeV	4 GeV

Table 14: List of cuts used in the $\widetilde{\mu}^+\widetilde{\mu}^-$ analysis. $E^{tag}_{\mu^\pm}$ is the isolated tagged (loose) $\mu^\pm$ energy. Isolation criteria corresponds to a 15 deg. cone around the tagged lepton with energy less than 10 GeV. The value y^{had}_{ij} corresponds to the durham resolution parameter for a flip from i jets to j jets configuration, (with i=j+1) whithout the two tagged muons.

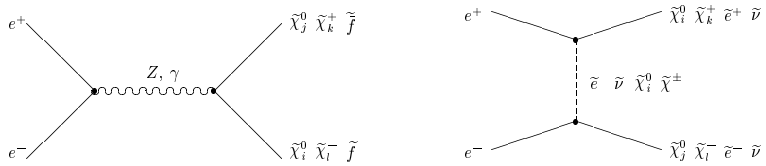

Figure 1: Neutralino, chargino and sfermion pair production diagrams ($i, j = 1, ..4$; $k, l = 1, 2$). Only charged partricles are produced via a γ in the s-channel

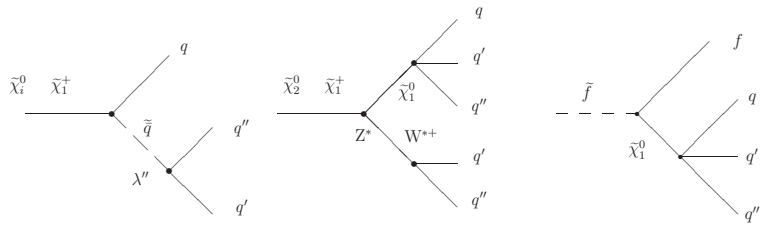

Figure 2: the two first diagrammes show $\widetilde{\chi}^0$ and $\widetilde{\chi}^\pm$ direct and indirect decay via λ'' coupling. The last one representes indirect decay of sfermions.

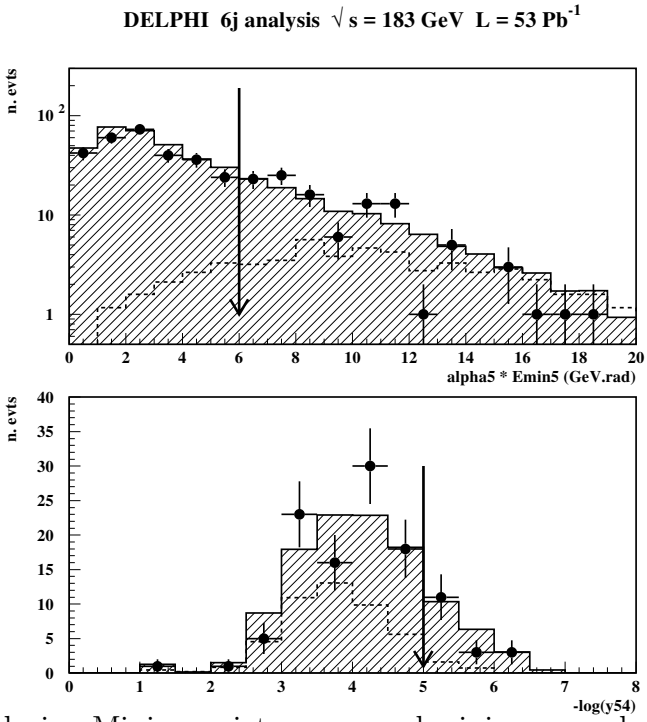

Figure 3: 6 jet analysis : Minimum jet energy and minimum angle in five jet configuration ($\alpha^5 E^5_{min}$ in rad.GeV) and the -Log of y_{54} for data (black dots) expected SM background (hatched) and $\widetilde{\chi}^0_1\widetilde{\chi}^0_1$ signal (dotted line) normalized to 2 pb. The arrows show applied cuts.

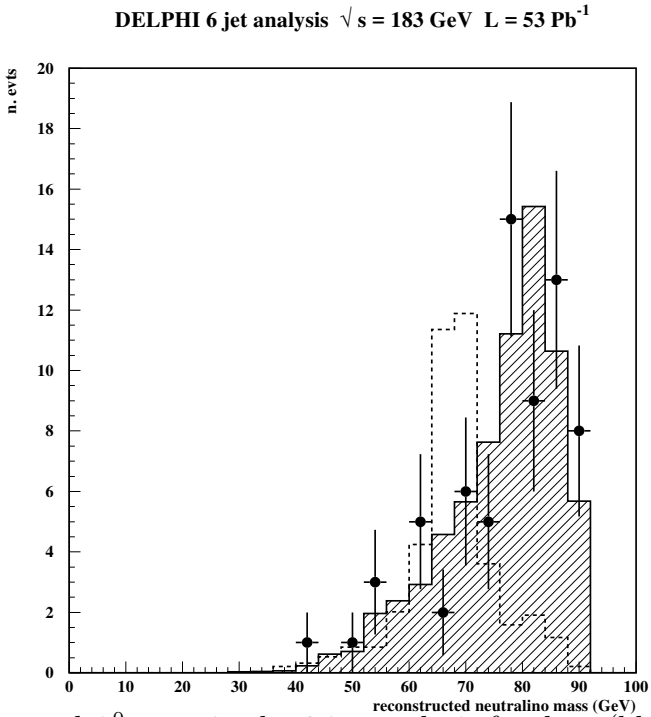

Figure 4: Reconstructed $\tilde{\chi}^0_1$ mass in the 6-jet analysis for data (black dots), expected SM background (hatched) and the signal (dotted line) with $m_{\tilde{\chi}^0_1} = 69$ GeV/c^2, normalized to 2 pb.

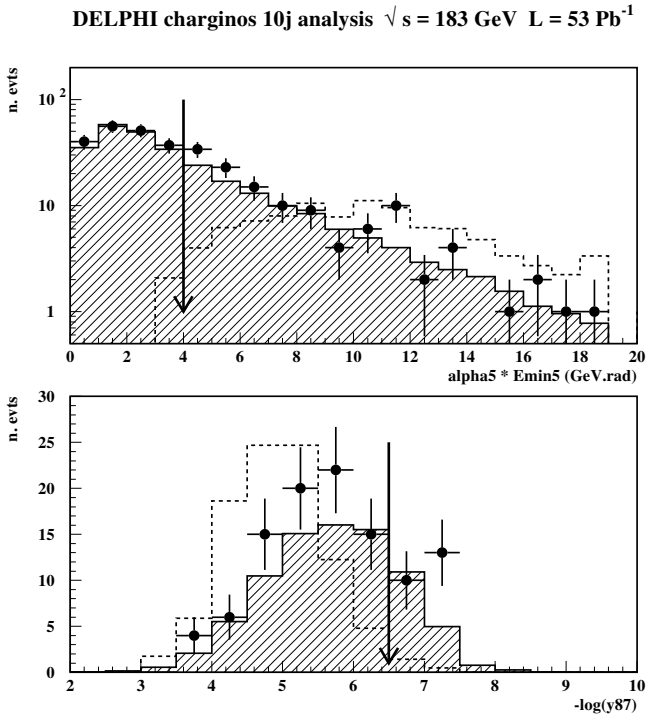

Figure 5: 10 jet analysis : Minimum jet energy and minimum angle in five jet configuration ($\alpha^5 E^5_{min}$ in rad.GeV) for Data (black dots) expected SM background (hatched) and $\widetilde{\chi}^0_1\widetilde{\chi}^0_1$ signal (dotted line) with $m_{\widetilde{\chi}^\pm} = 69$ GeV/c^2) and $m_{\widetilde{\chi}^0} = 38$ GeV/c^2 normalized to 1 pb. The second plot show the jet resolution parameter in 8 jet configuration. The arrows show applied cuts.

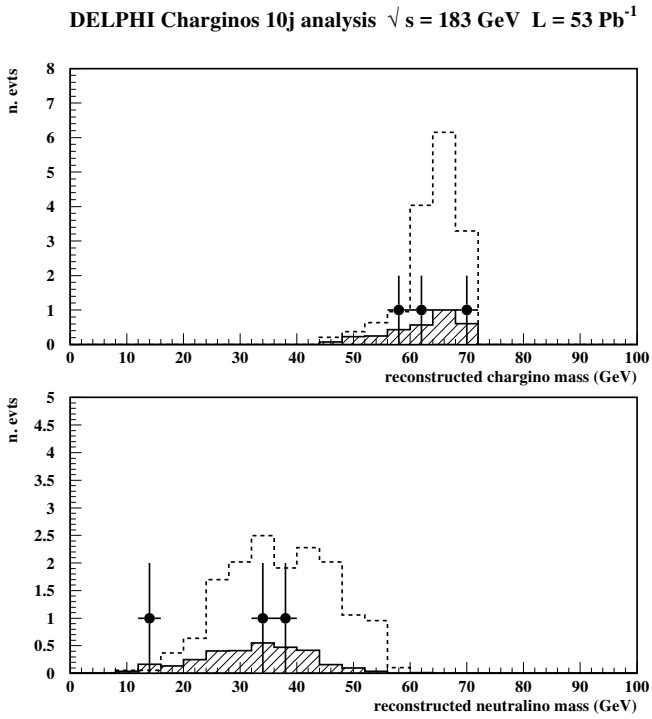

Figure 6: Reconstructed $\tilde{\chi}_1^0$ and $\tilde{\chi}_1^+$ masses for real data (black dots) expected SM background (hatched) and $\widetilde{\chi}_1^0\widetilde{\chi}_1^0$ signal (dotted line) with $m_{\tilde{\chi}^\pm} = 69$ GeV/c^2 and $m_{\tilde{\chi}^0} = 38$ GeV/c^2), normalized to 1 pb.

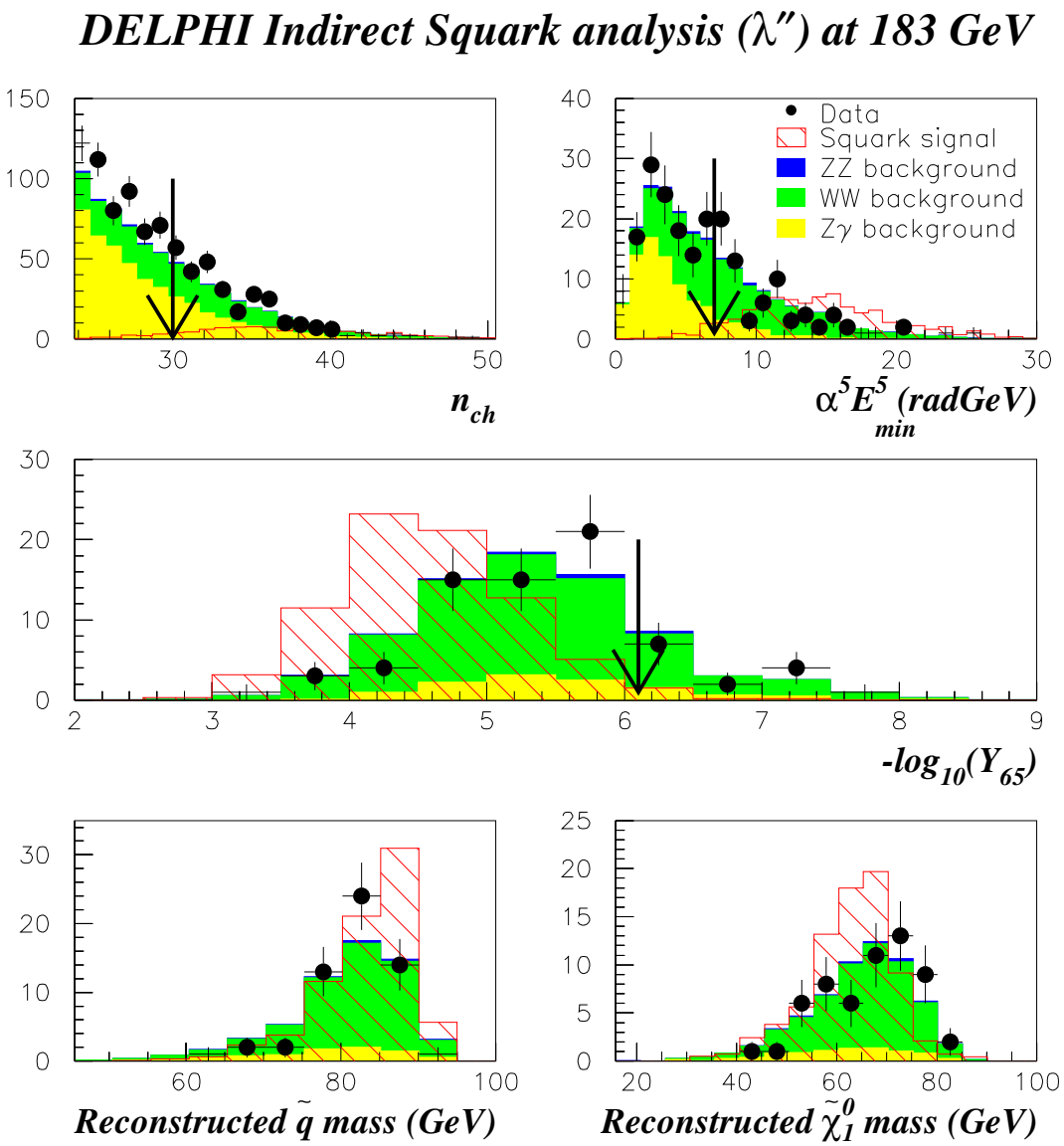

Figure 7: Plots illustrating selection cuts and mass reconstruction in the indirect squark analysis of the 53 pb^{-1} of DELPHI data at 183 GeV, SM backgrounds and a simulated signal of 2 pb. The SUSY signal was generated at $m_{\tilde{q}} = 85$ GeV and $m_{\tilde{\chi}^0_1} = 60$ GeV and decays indirectly through an R-parity violating $\bar{U}\bar{D}\bar{D}$ coupling. The arrows indicate applied selection criteria (see table 12).

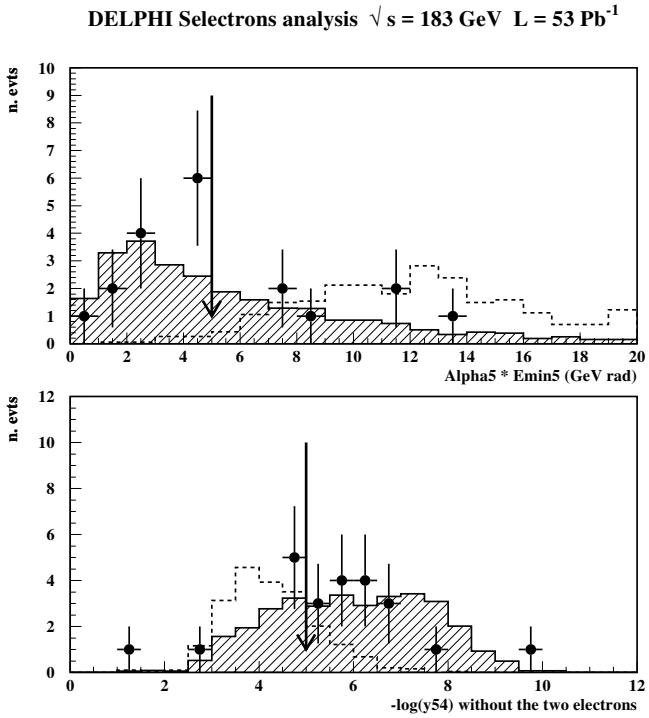

Figure 8: Selectrons analysis : Minimum jet energy and minimum angle in five jet configuration ($\alpha^5 E^5_{min}$ in rad.GeV) and -Log of the hadronic y^{had}_{54} resolution parameter for data (black dots) expected SM background (hatched) and $\widetilde{\chi}^0_1\widetilde{\chi}^0_1$ signal (dotted line) normalized to 1 pb. The arrows show applied cuts.

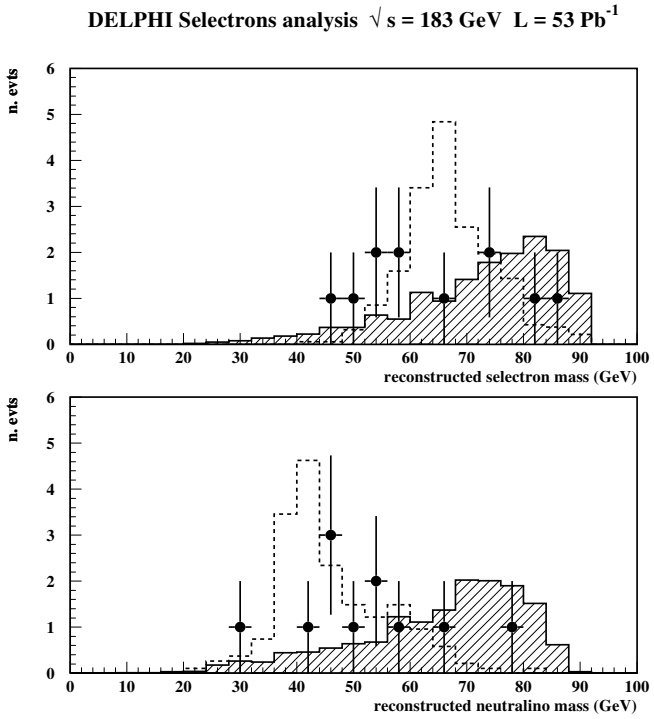

Figure 9: Reconstructed $\widetilde{e}$ and $\tilde{\chi}^0_1$ mass in the selectron analysis for data (black dots), expected SM background (hatched) and the signal (dotted line) with $m_{\tilde{e}^{\pm}} = 65$ GeV/c^2) and $m_{\tilde{\chi}^0} = 40$ GeV/c^2), normalized to 1 pb.

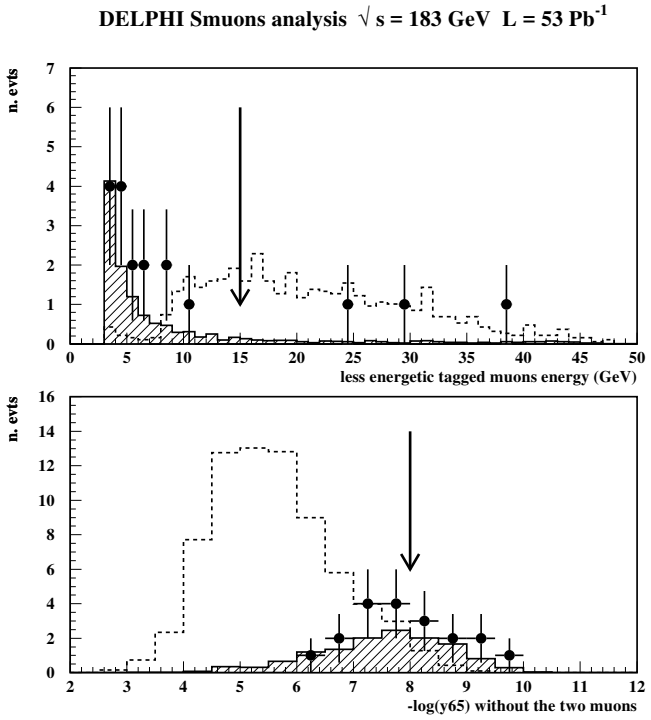

Figure 10: 10 jet analysis : Energy of the lowest energetic tagged muons and the -Log of the hadronic y_{65}^{had} resolution parameter for data (black dots) expected SM background (hatched) and $\widetilde{\chi}_1^0\widetilde{\chi}_1^0$ signal (dotted line) normalized to 1 pb. The arrows show applied cuts.

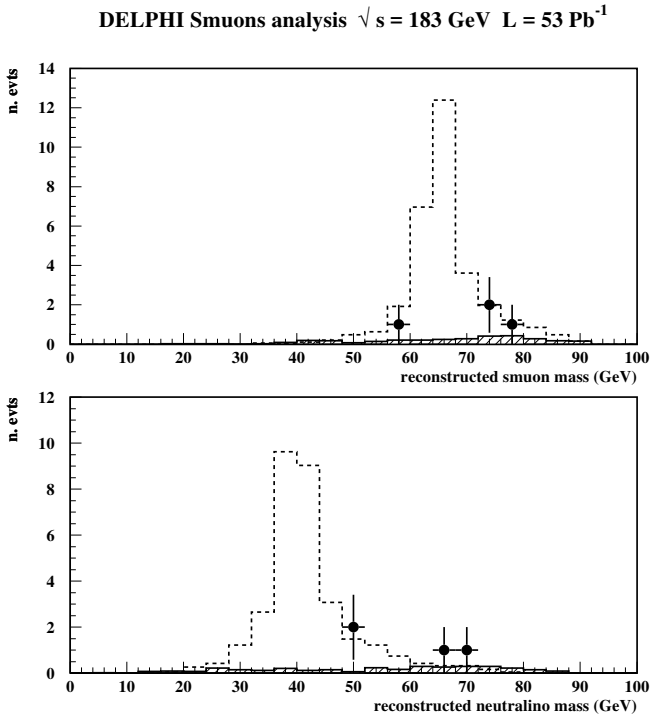

Figure 11: Reconstructed $\widetilde{\mu}$ and $\tilde{\chi}^0_1$ mass in the smuons analysis for data (black dots), expected SM background (hatched) and the signal (dotted line) with $m_{\tilde{\mu}^\pm} = 65$ GeV/c^2) and $m_{\tilde{\chi}^0} = 40$ GeV/c^2), normalized to 1 pb.

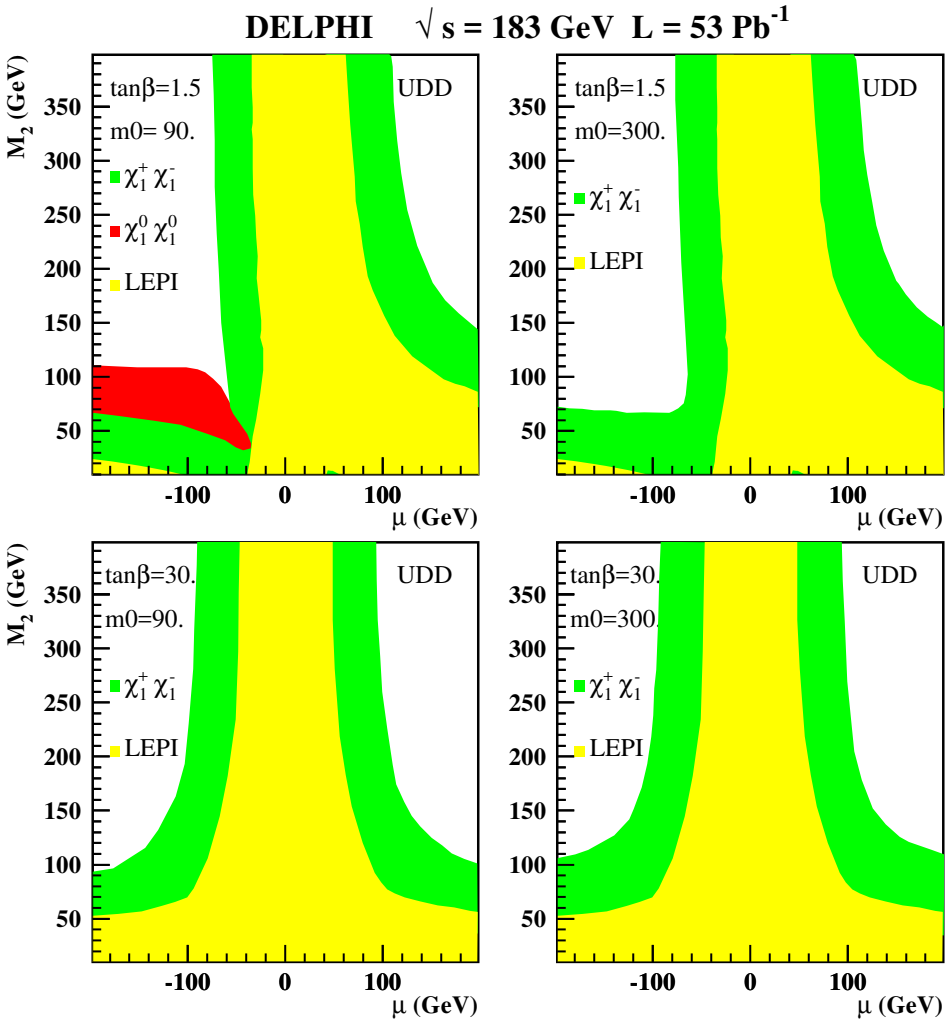

Figure 12: exclusion plot in μ, M_2 plan for $\tilde{\chi}_1^0\ \tilde{\chi}_1^0$ and $\tilde{\chi}_1^+\ \tilde{\chi}_1^-$ production in the case of a dominant UDD R-parity violation coupling.

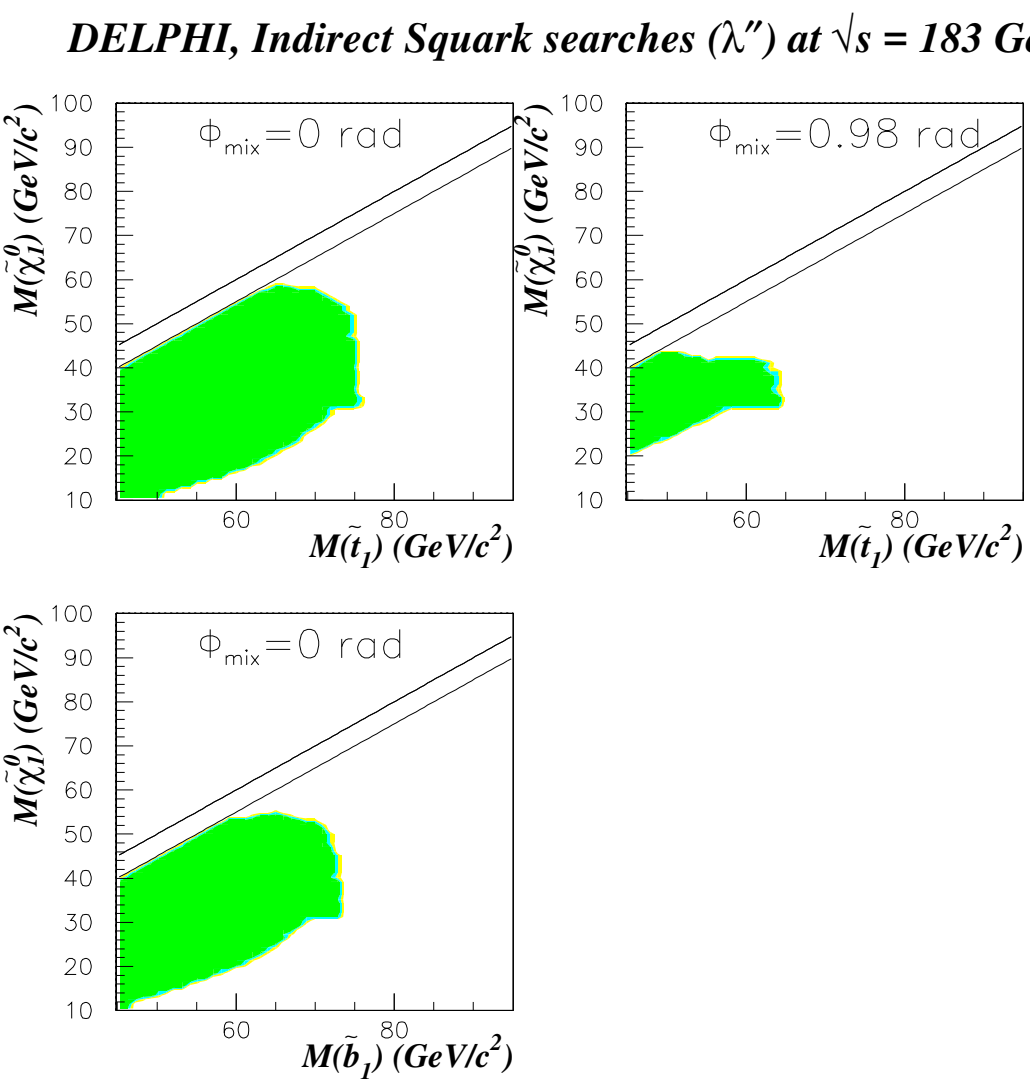

Figure 13: Exclusion domains at 95% confidence level in the $M(\tilde{\chi}_1^0)$, $M(\tilde{q})$ plane for indirectly decaying squarks in the case of a dominant R-parity violation $\bar{U}\bar{D}\bar{D}$ coupling. The plots to the left show the exclusion for pure left handed stop and sbottom respectively. The upper right plot shows the exclusion for a stop with a minimum cross section producing mixing angle. The two diagonal lines indicate the degenerate mass region (0 GeV$\leq M(\tilde{q}) - M(\tilde{\chi}_1^0) \leq$ 5 GeV), above which indirect squark decays are kinematically forbidden.

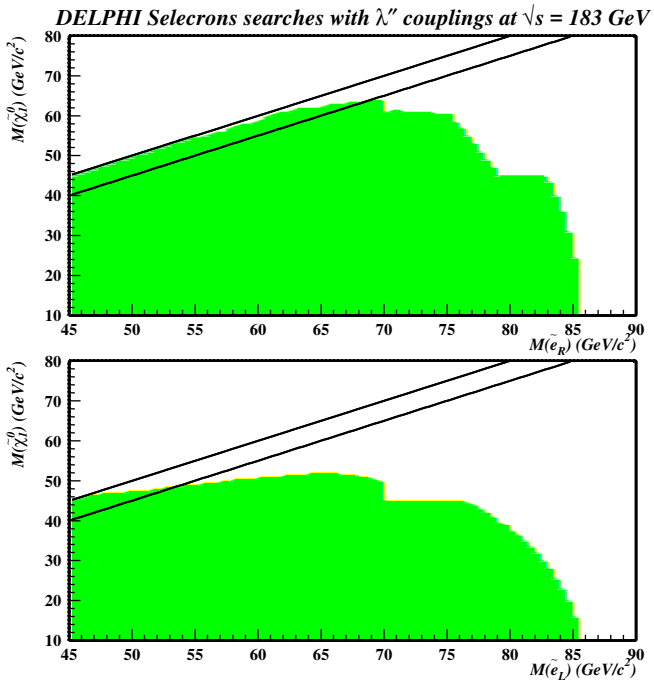

Figure 14: Exclusion domains at 95% confidence level in the $M(\tilde{\chi}_1^0)$, $M(\tilde{e})$ plane for indirectly decaying selectron in the case of a dominant R-parity violation $\bar{U}\bar{D}\bar{D}$ coupling. The upper (lower) plot shows the exclusion for pure right (left) handed selectron. The two diagonal lines indicate the degenerate mass region (0 GeV$\leq M(\tilde{e}) - M(\tilde{\chi}_1^0) \leq$ 5 GeV).

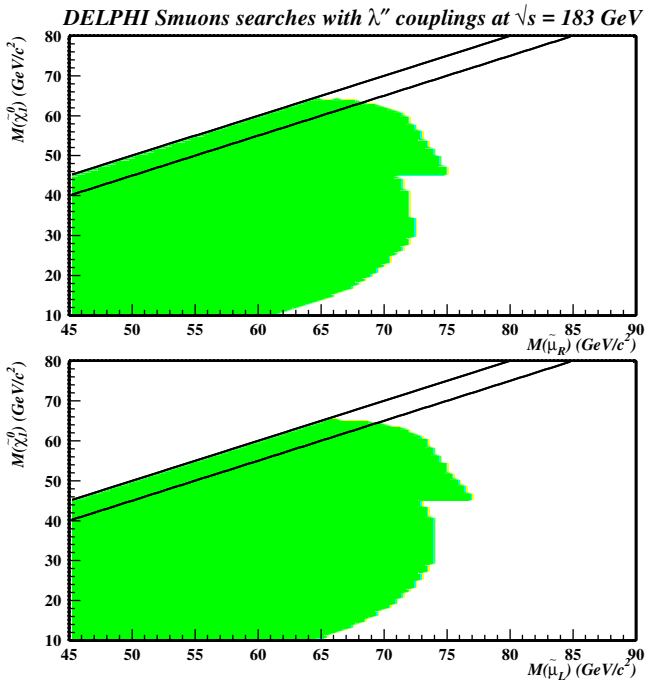

Figure 15: Exclusion domains at 95% confidence level in the $M(\tilde{\chi}_1^0)$, $M(\tilde{\mu})$ plane for indirectly decaying selectron in the case of a dominant R-parity violation $\bar{U}\bar{D}\bar{D}$ coupling. The upper (lower) plot shows the exclusion for pure right (left) handed smuon. The two diagonal lines indicate the degenerate mass region (0 GeV$\leq M(\tilde{\mu}) - M(\tilde{\chi}_1^0) \leq$ 5 GeV).